Acta Pharmacologica Sinica

www.nature.com/aps

ARTICLE

Satellite cell-derived exosome-mediated delivery of microRNA-23a/27a/26a cluster ameliorates the renal tubulointerstitial fibrosis in mouse diabetic nephropathy

Jia-ling Ji[1], Hui-min Shi[1], Zuo-lin Li[2], Ran Jin[1], Gao-ting Qu[1], Hui Zheng[1], E. Wang[1], Yun-yang Qiao[1], Xing-yue Li[1], Ling Ding[3], Da-fa Ding[4], Liu-cheng Ding[5], Wei-hua Gan[1], Bin Wang[2]✉ and Ai-qing Zhang[3]✉

Renal tubulointerstitial fibrosis (TIF) is considered as the final convergent pathway of diabetic nephropathy (DN) without effective therapies currently. MiRNAs play a key role in fibrotic diseases and become promising therapeutic targets for kidney diseases, while miRNA clusters, formed by the cluster arrangement of miRNAs on chromosomes, can regulate diverse biological functions alone or synergistically. In this study, we developed clustered miR-23a/27a/26a-loaded skeletal muscle satellite cells–derived exosomes (Exos) engineered with RVG peptide, and investigated their therapeutic efficacy in a murine model of DN. Firstly, we showed that miR-23a-3p, miR-26a-5p and miR-27a-3p were markedly decreased in serum samples of DN patients using miRNA sequencing. Meanwhile, we confirmed that miR-23a-3p, miR-26a-5p and miR-27a-3p were primarily located in proximal renal tubules and highly negatively correlated with TIF in *db/db* mice at 20 weeks of age. We then engineered RVG-miR-23a/27a/26a cluster loaded Exos derived from muscle satellite cells, which not only enhanced the stability of miR-23a/27a/26a cluster, but also efficiently delivered more miR-23a/27a/26a cluster homing to the injured kidney. More importantly, administration of RVG-miR-23a/27a/26a-Exos (100 μg, i.v., once a week for 8 weeks) significantly ameliorated tubular injury and TIF in *db/db* mice at 20 weeks of age. We revealed that miR-23a/27a/26a-Exos enhanced antifibrotic effects by repressing miRNA cluster-targeting Lpp simultaneously, as well as miR-27a-3p-targeting Zbtb20 and miR-26a-5p-targeting Klhl42, respectively. Knockdown of Lpp by injection of AAV-Lpp-RNAi effectively ameliorated the progression of TIF in DN mice. Taken together, we established a novel kidney-targeting Exo-based delivery system by manipulating the miRNA-23a/27a/26a cluster to ameliorate TIF in DN, thus providing a promising therapeutic strategy for DN.

Keywords: diabetic nephropathy; tubulointerstitial fibrosis; skeletal muscle satellite cell; exosomes; miR-23a/27a/26a cluster; Lpp; Zbtb20; Klhl42

Acta Pharmacologica Sinica (2023) 44:2455–2468; https://doi.org/10.1038/s41401-023-01140-4

INTRODUCTION

Diabetic nephropathy (DN), a common and severe complication of diabetes mellitus (DM), has become the leading cause of end-stage renal disease (ESRD) [1]. Growing evidence indicates that renal tubulointerstitial fibrosis (TIF) is the best indicator of deterioration of renal function in DN and is highly positively correlated with the progression of DN [2, 3]. However, there remain no definitive therapies for TIF to prevent DN from progressing to ESRD.

MicroRNAs (miRNAs), a class of evolutionarily conserved and endogenous noncoding RNAs, play indispensable roles in the pathophysiology of human diseases at the post-transcriptional level [4]. Convincing evidence has shown that miRNAs play a key role in fibrotic diseases and may become promising therapeutic targets for kidney diseases [5–7]. However, given the poor therapeutic effect of applying a single miRNA owing to biological complexity and inefficient delivery in vivo, miRNA clusters, usually formed by the cluster arrangement of miRNAs on chromosomes, were proposed to provide therapeutically relevant epigenetic interference [8]. Functionally, these clustered miRNAs can regulate diverse biological functions alone or synergistically. Previous studies have revealed that miRNA clusters have more advantages than single miRNA [9, 10]. However, the potential therapeutic effect of miRNA clusters in DN remains unclear. Effective improvement in miRNA cluster stability and selective targeting of the kidney are also urgently needed.

Exosomes (Exos), secreted by almost all types of cells, mediate cell-cell communications, and cell-environment interactions by transferring a variety of biologically active components [11, 12]. Previous studies have revealed that Exos can stabilize miRNAs and, due to their endogeneity and heterogeneity, can be used as stable nanocarriers to deliver drugs and exogenous genes for the

[1]Department of Pediatric Nephrology, the Second Affiliated Hospital of Nanjing Medical University, Nanjing 210003, China; [2]Institute of Nephrology, Zhong Da Hospital, Southeast University School of Medicine, Nanjing 210009, China; [3]Department of Pediatrics, the Fourth Affiliated Hospital of Nanjing Medical University, Nanjing 210031, China; [4]Department of Endocrinology, the Second Affiliated Hospital of Nanjing Medical University, Nanjing 210003, China and [5]Department of Urology, the Second Affiliated Hospital of Nanjing Medical University, Nanjing 210003, China
Correspondence: Bin Wang (wangbinhewei@126.com) or Ai-qing Zhang (njaiqing@njmu.edu.cn)
These authors contributed equally: Jia-ling Ji, Hui-min Shi, Zuo-lin Li

Received: 26 March 2023 Accepted: 12 July 2023
Published online: 18 August 2023

treatment of various diseases [13–15]. Recently, Kim et al. reported that the use of Exos as a delivery system for the super-repressor IκBα could ameliorate ischemia-reperfusion-induced acute kidney injury [16]. In addition, as a nanotherapeutic vector, Exos can transport specific miRNAs to injured kidneys to ameliorate renal fibrosis [17]. Thus, an Exo-based delivery system may be a promising candidate to manipulate miRNA clusters for the effective treatment of TIF.

In recent years, increasing evidence has demonstrated that stem cell Exo-based therapy is an exciting approach for a variety of human diseases [18, 19] and has the advantages of a strong targeting ability and low immunogenicity. At present, multiple stem cell Exo-based therapies have achieved promising results in animal models of kidney disease [20, 21]. Skeletal muscle satellite cells, a class of muscle stem cells, show self-renewal in response to tissue injury [22, 23]. Our previous studies also found that satellite cell-derived Exos carrying miR-29 could prevent renal fibrosis in obstructive nephropathy, in which the rabies virus glycoprotein (RVG) peptide engineered to localize at the surface of Exos through fused protein Lamp2b (lysosome-associated membrane glycoprotein 2b) was also employed to home to the injured kidneys by realizing specific targeting [24]. Thus, we speculated that satellite cell-derived Exos encapsulating specific miRNA clusters provide a novel therapeutic strategy for the treatment of TIF in DN.

Here, we successfully engineered RVG-miR-23a/27a/26a cluster-loaded Exos derived from muscle satellite cells and investigated their therapeutic efficacy in a murine model of DN. Interestingly, we found that RVG-miR-23a/27a/26a-Exos not only enhanced the stability of the miR-23a/27a/26a cluster but also efficiently delivered more miR-23a/27a/26a clusters homing to the injured kidneys. More importantly, treatment with RVG-miR-23a/27a/26a-Exos significantly ameliorated tubular injury and TIF in mice with DN. Together, our findings strongly supported the use of satellite cell-derived Exos as a versatile delivery system for the miR-23a/27a/26a cluster as an effective strategy for the treatment of TIF in DN.

MATERIALS AND METHODS

Human serum samples

Human serum samples from patients with DM and DN were obtained from the Department of Endocrinology, the Second Affiliated Hospital of Nanjing Medical University. This study was approved by the Ethics Committee of Nanjing Medical University [No. (2022)-KY-037-01], and written informed consent was obtained from all patients. Inclusion criteria: Eligible patients with DN, had a history of DM and urinary albumin/creatinine ratio ≥300 mg/g, as well as an estimated glomerular filtration rate ≤60 mL·min^{-1} (1.73 m^2)$^{-1}$ [25]. All information about the human subjects is summarized in Supplementary Table S1.

Primary skeletal muscle satellite cell culture

All male 4-week-old C57BL/6 mice weighing 15–16 g were purchased from GemPharmatech LLC (Nanjing, China). Primary skeletal muscle satellite cells were dissociated from limb muscles of 4-week-old mice and isolated from skeletal muscle tissue using a Skeletal Muscle Dissociation Kit (130-098-305, MACS, Miltenyi Biotec, Inc., Germany) and a Satellite Cell Isolation Kit (130-104-267, MACS, Miltenyi Biotec, Inc., Germany) [24]. Isolated satellite cells were cultured in expansion medium containing 40% Dulbecco's modified Eagle's medium (DMEM, C11995500BT, Gibco, CA, USA), 40% Ham's F10 (318-050-CL, Wisent Corporation, Canada), 20% fetal bovine serum (FBS, 10099-141, Gibco, CA, USA), 2.5 ng/mL human fibroblast growth factor-2 (FGF-2, HY-P7331, MedChemExpress, NJ, USA) and 100 U/mL penicillin/streptomycin (15140-122, Gibco, CA, USA) according to the manufacturer's protocol. After six days, the cells were cultured in differentiation medium without FGF-2 for three days. Satellite cells were stained with anti-Desmin (AF5334, Affinity Biosciences, MICH, USA) to identify purification by immunofluorescence. The animal experiment was performed in accordance with the ARRIVE guidelines and the National Institutes of Health Guide for the Care and Use of Laboratory Animals, and was approved by the Institutional Animal Care and Use Committee of Nanjing Medical University (No. 2104020).

Preparation and characterization of RVG-miR-23a/27a/26a-Exos

An adenovirus (Ad) carrying the miR-23a/27a/26a cluster (hereinafter referred to as cluster 3) or RVG-Lamp2b was purchased from Genechem Co., Ltd (Shanghai, China) and transfected into satellite cells. Briefly, satellite cells were prepared and transfected with Ad-cluster 3 (1×10^9) and Ad-RVG-Lamp2b (1×10^9) with FBS-free medium. After 12 h of transfection, the medium was replaced with complete medium for 48 h. Subsequently, the supernatants were collected and centrifuged at $2000 \times g$ for 20 min and $13{,}500 \times g$ for 25 min and then ultracentrifuged at $200{,}000 \times g$ for 2 h (Optima L-80 XP, Beckman, CA, USA) at 4 °C according to our previous experiments [15]. Similarly, RVG-miR-26a-Exos, RVG-miR-23a/27a-Exos and RVG-vector-Exos were produced following the same method. The Exos pellets were resuspended in sterile phosphate buffer saline (PBS, C10010500BT, Gibco, CA, USA) and stored at −80 °C. The size and concentration of Exos were detected by Nanoparticle Tracking Analysis (NTA, ZetaView PMX 110, Particle Metrix, Meerbusch, Germany). The morphology of Exos was observed under Transmission Electron Microscope (TEM, Hitachi, Japan). Exosomal surface markers, including Alix, CD63 and CD81, were analyzed by Western blot.

Exos distribution in vivo

For analysis of in vivo Exos distribution, DiD-labeled Exos were produced first. Satellite cells were incubated with DiD (C1039, Beyotime Biotechnology, Shanghai, China) for 20 min. The final concentration of DiD was 5 μM. Then, the cells were washed with PBS twice to remove excess dye. After being cultured with FBS-free medium for 48 h, the supernatants were collected, and Exos were isolated according to the procedure described above. Furthermore, DiD-labeled Exos were injected intravenously into *db/m* and *db/db* mice, and kidneys were excised and imaged using the IVIS Spectrum imaging system (PerkinElmer, MA, USA).

Animal models and therapeutic experiments

The study protocols were reviewed and approved by the Institutional Animal Care and Use Committee of Nanjing Medical University (No. 2104020). Experiments were conducted using 8-week-old male C57BLKS/J^{Lepr} background *db/db* mice (43–45 g) as a type 2 diabetes model and their age-matched heterozygous male *db/m* mice as a control purchased from GemPharmatech LLC (Nanjing, China). The *db/db* mice developed hyperglycemia from approximately 8 weeks of age at 9.7 ± 1.6 mM, with a progressive increase in hyperglycemia of more than 28.6 ± 13.2 mM by 20 weeks of age [26]. Moreover, renal hypertrophy was evaluated at 20 weeks of age, and renal function was worsened, accompanied by glomerular enlargement, diffuse expansion of mesangial matrix and TIF [27]. Thus, *db/db* mice are an invaluable tool for the study of human DN. These mice were randomly divided into several groups according to the experimental protocol and were allowed free access to the same diet under the same conditions. At 12 weeks of age, *db/db* mice were separately intravenously administered PBS, RVG-cluster 3-Exos, RVG-miR-26a-Exos, RVG-miR-23a/27a-Exos or RVG-vector-Exos by the tail vein once a week for 8 weeks ($n = 7$ per group and 100 μg Exos). All mice were euthanized by intraperitoneal injection of barbital sodium (100 mg/kg) at 20 weeks of age. Blood, 24 h urine and renal parenchyma specimens were collected for further experiments.

Adeno-associated virus (AAV)-treated mice
For AAV9-mediated lipoma-preferred partner (Lpp) knockdown in mice, AAV was developed and obtained from Genechem Co., Ltd. (Shanghai, China). For Lpp knockdown experiments, *db/db* mice were randomly divided into two groups: *db/db* + AAV-Lpp-RNAi and *db/db* + AAV-NC ($n = 5$ per group). The *db/db* mice received a single injection by tail vein with AAV-Lpp-RNAi or AAV-NC (1×10^{12} viral genomes). After 4 weeks, renal function and its related indicators were measured.

Renal tubular epithelial cells (TECs) culture
Primary mouse TECs were isolated from the kidneys of 8-week-old male C57BL/6 mice [28]. Briefly, all mice were euthanized by intraperitoneal injection of barbital sodium (100 mg/kg), and the kidneys were harvested. The cortical tissue was cut into 2–4 mm pieces and digested in 0.75 mg/mL collagenase for 1 h at 37 °C. Subsequently, the digested tissue was filtered using a smart strainer and centrifuged at 5000 r/min for 20 min. Finally, the cells were suspended in DMEM containing 10% FBS and 1% penicillin/streptomycin. Cells were seeded in 12-well plates and treated with high glucose (HG, 30 mM) or normal glucose (control, 5.5 mM). D-Mannitol (5.5 mM glucose + 24.5 mM mannitol) was chosen as a control for osmolality. After 48 h of treatment, the cells were harvested for subsequent experiments. The animal experiment was performed in accordance with the ARRIVE guidelines and the National Institutes of Health Guide for the Care and Use of Laboratory Animals and approved by the Institutional Animal Care and Use Committee of Nanjing Medical University (No. 2104020).

Cellular uptake of Exos in vitro
TECs were seeded evenly on confocal dishes and then incubated with DiD-labeled Exos when grown to approximately 70% confluence. After 48 h, the cells were washed with PBS three times and fixed with 4% paraformaldehyde for 20 min. Subsequently, DiD-positive cells were analyzed by confocal microscopy.

Quantitative real-time polymerase chain reaction (qRT–PCR) analysis
Total RNA was extracted using TRIzol (15596018, Invitrogen, CA, USA). The level of mRNA was quantified with HiScript III RT SuperMix (R323, Vazyme Biotech Co., Ltd, Nanjing, China), and the level of miRNA was detected with the All-in-One MicroRNA Assay Kit (QP011, GeneCopoeia, MD, USA) under the StepOne Real Time PCR System (Applied Biosystems, CA, USA). The thermocycling conditions for qRT–PCR were performed according to established protocols [29]. All primers involved in this study were obtained from Generay Biotech Co., Ltd. (Shanghai, China). GAPDH and U6 were used as the internal controls for normalization. Cel-miR-39-3p was used as the control. The sequences of the primers used are listed in Supplementary Table S2.

Western blot
Total protein samples from exosomes, cells and kidney tissues were harvested with RIPA lysis buffer (P0013B, Beyotime Biotechnology, Shanghai, China), and the concentration was determined using a BCA assay (P0010, Beyotime Biotechnology, Shanghai, China). Equal amounts of proteins were separated by 8% or 10% SDS–PAGE (E302-01 and E303-01, Vazyme Biotech Co., Ltd, Nanjing, China) and transferred onto 0.45 μm PVDF membranes (IPVH00010, Millipore, CA, USA). Western blot was performed as previously described [30]. Immunoblotting was performed with the following primary antibodies: anti-GAPDH (AF7021, Affinity Biosciences, MICH, USA), anti-CD63 (sc-5275, Santa Cruz, CA, USA), anti-Alix (sc-53540, Santa Cruz, CA, USA), anti-CD81 (10037, Cell Signaling Technology, MA, USA), anti-Lamp2b (ab25631, Abcam, UK), anti-α-smooth muscle actin (α-SMA, AF1032, Affinity Biosciences, MICH, USA), anti-collagen I (ab138492, Abcam, UK), anti-Fibronectin (ab2413, Abcam, UK), anti-E-cadherin (AF0131, Affinity Biosciences, MICH, USA), anti-kidney injury molecule-1 (Kim-1, MA5-28211, Thermo Fisher Scientific, MA, USA), anti-Lpp (sc-101434, Santa Cruz, CA, USA), anti-zinc finger and BTB domain containing 20 (Zbtb20, sc-515370, Santa Cruz, CA, USA), and anti-kelch-like protein 42 (Klhl42, 24847-1-AP, Proteintech, CA, USA). The secondary HRP-conjugated antibodies were anti-mouse IgG and anti-rabbit IgG obtained from KeyGEN BioTECH (Nanjing, China). Intensity values expressed as the relative protein expression were analyzed by ImageJ software 1.8.0 and normalized to the expression of GAPDH.

Immunofluorescence staining and immunohistochemistry
Four-micrometer-thick paraffin-embedded renal tissue sections were prepared, and a streptavidin peroxidase detection system (Maixin, Fuzhou, China) was used for immunofluorescence staining and immunohistochemistry assays. All experimental steps followed the manufacturer's protocol. Tissue sections were incubated with primary antibodies against α-SMA, Kim-1, Lpp, Zbtb20, Desmin and Klhl42. Immunostained samples were visualized under a confocal microscope (FV1000, Olympus, Japan).

Luciferase reporter assay
HEK293T cells were seeded into 24-well plates and the confluence reaches to 50% after incubation. miR-23a-3p mimic, miR-27a-3p mimic, miR-26a-5p mimic, 3′UTR-Lpp-WT, 3′UTR-Lpp-MUT, 3′UTR-Zbtb20-WT, 3′UTR-Zbtb20-MUT, 3′UTR-Klhl42-WT and 3′UTR-Klhl42-MUT were purchased from Guangzhou RiboBio Co., Ltd (Guangzhou, China). As Lpp was predicted target of miR-23a-3p, HEK293T cells were co-transfected with miR-23a-3p mimic (20 μM) or miR-NC (20 μM) together with 3′UTR-Lpp-WT (100 ng) or 3′UTR-Lpp-MUT (100 ng) reporter plasmids using Lipofectamine 2000 (Thermo Fisher Scientific, MA, USA) according to the manufacturer's instruction. After transfection for 48 h, the luciferase activity of cells was measured by a Dual Luciferase Assay Kit (E1910, Promega, WI, USA) and microplate reader (Tecan M1000, Switzerland). Similarly, the targeting relationship between miR-26a-5p and Lpp, miR-26a-5p and Klhl42, as well as miR-27a-3p and Zbtb20, were verified using the above method.

Fluorescence in situ hybridization (FISH)
FISH kit (GenePharma, Shanghai, China) was used to determine the location of miR-23a-3p, miR-26a-5p and miR-27a-3p in TECs. Cy3-labeled probes of miR-23a-3p, miR-26a-5p and miR-27a-3p were obtained from GenePharma (Shanghai, China). Four-micrometer-thick paraffin-embedded tissue sections were digested with protease K and then incubated with blocking buffer for 30 min at 37 °C. Furthermore, the tissue sections were hybridized with Cy3-labeled DNA probe sets at 37 °C overnight. FISH images were observed under a fluorescence microscope.

Correlation analysis
For determination of the association between miR-23a-3p, miR-26a-5p, and miR-27a-3p and TIF, correlation analysis was applied using Pearson's correlation. According to the classification for Pearson's correlation coefficient (r), "$r = 0$" indicated "no correlation", "$r < 0.3$" represented "poor correlation", "$0.3 \le r < 0.5$" was treated as "moderate correlation", "$0.5 \le r < 0.7$" was regarded as "good correlation", "$r \ge 0.7$" indicated "strong correlation" and "$r = 1$" represented "perfect correlation".

Statistical analysis
Data are expressed as the mean ± SEM. Statistical analyses were performed using SPSS 22.0. All experiments were repeated three times. When two groups were compared, an unpaired t test was used. When three or more groups were compared, one-way ANOVA followed by Bonferroni's correction was employed to analyze the differences. Statistical significance was set at $P < 0.05$.

RESULTS

Downregulated miR-23a-3p, miR-26a-5p, and miR-27a-3p were associated with TIF in DN

To identify the potential therapeutic targets for DN, serum samples from patients with DN were analyzed using high-throughput miRNA sequencing (miRNA-seq). MiRNA expression profiles differed substantially and were displayed by a hierarchical clustering heatmap (Fig. 1a). A total of 23 differentially expressed miRNAs with fold change >2.0 and *P* value <0.05 were identified (six downregulated and seventeen upregulated) (Supplementary Table S3). In the miRNA-seq results, we were surprised to find that miR-23a-3p, miR-26a-5p, and miR-27a-3p were significantly decreased (Supplementary Table S3). Notably, miR-23a-3p and miR-27a-3p are located in a cluster (miR-23a~27a cluster) on chromosome 9q22 in humans [31]. Then, we confirmed that miR-23a-3p, miR-26a-5p, and miR-27a-3p expression in the serum of patients with DN was reduced by 47%, 57% and 38%, respectively (Fig. 1b). Moreover, our previous studies have demonstrated that miR-23a-3p and miR-27a-3p can attenuate renal fibrosis and muscle atrophy in a 5/6 nephrectomy mouse model [32, 33] and that miR-26a-5p plays an important role in anti-renal fibrosis in obstructive kidney disease [30]. Therefore, miR-23a-3p, miR-26a-5p, and miR-27a-3p were further investigated.

Then, to investigate the correlation between miR-23a-3p, miR-26a-5p, miR-27a-3p and TIF in DN, we established a type 2 diabetic model with *db/db* mice to resemble human diabetic kidney disease in our study. As shown in Fig. 1c, there were markedly elevated levels of serum creatinine (sCr) and 24 h urinary protein in the *db/db* mice at 20 weeks of age. Histologically, significant vacuolar degeneration of tubules and interstitial fibrosis were observed in the DN group (Fig. 1d, e). Moreover, the expression of the fibrotic markers α-SMA, collagen I, Fibronectin, and the tubular injury marker Kim-1 were markedly increased, while the expression of E-cadherin was decreased (Supplementary Fig. S1a, b). Consistently, the immunohistochemistry results showed upregulation of α-SMA and Kim-1 in the DN group (Supplementary Fig. S1c). Furthermore, the results of FISH analysis showed that miR-23a-3p, miR-26a-5p, and miR-27a-3p were primarily located in lotus tetragonolobus lectin (LTL^+) proximal renal tubules (Fig. 1f) and were consistently reduced in the DN group, as shown by qRT–PCR (Fig. 1g). Furthermore, correlations between the three miRNAs and TIF were evaluated using Pearson's correlation analysis. As listed in Fig. 1h, the results of correlation analysis demonstrated that there was a strong negative correlation between miR-23a-3p ($r = 0.8066$), miR-26a-5p ($r = 0.8509$), miR-27a-3p ($r = 0.8735$) and TIF. In addition, miR-23a-3p, miR-26a-5p, and miR-27a-3p were found to be strongly negatively correlated with renal function decline (Supplementary Fig. S1d) and 24 h urinary protein (Supplementary Fig. S1e). Here, we combined miR-23a-3p, miR-26a-5p, and miR-27a-3p into an artificially engineered cluster 3 and investigated their role in TIF in DN.

Engineered RVG-modified Exos targeted injured kidneys

To enhance the stability of the cluster 3 and deliver more cluster 3 homing to the injured kidneys, we generated satellite cell-derived RVG-cluster 3-Exos. In brief, we transfected satellite cells with Ad encoding RVG-Lamp2b and cluster 3, followed by Exos purification (Fig. 2a). Cultured satellite cells were identified by optical microscopy and immunofluorescence staining with a primary antibody against Desmin, a satellite cell surface marker protein (Supplementary Fig. S2a). Then, Exos isolated and purified from the supernatant of cultured cells were characterized by TEM, NTA and Western blot. TEM analysis showed that the Exos were typical lipid bilayer vesicles (Fig. 2b). NTA analysis verified that the size distribution peak of the Exos was 120 nm in diameter (Fig. 2c). The isolated Exos expressed Exo-associated markers (Alix, CD63, and CD81) as shown by Western blot (Fig. 2d). Furthermore, Western blot analysis showed that RVG-Lamp2b overexpression significantly increased Lamp2b expression in Exos (Supplementary Fig. S2b), which indicated that RVG-Lamp2b was incorporated into satellite cell-derived Exos. Overexpressed cluster 3 was confirmed to be incorporated into Exos, as evidenced by the fact that miR-23a-3p, miR-26a-5p, and miR-27a-3p expression levels were markedly elevated in the RVG-cluster 3-Exo group compared to the RVG-vector-Exo group (Fig. 2e). These data indicated that the strategy to establish RVG-cluster 3-Exos is valid.

Furthermore, we determined the stability of RVG-cluster 3-Exos and noted that no obvious degradation occurred in the miR-23a-3p, miR-26a-5p, and miR-27a-3p levels within Exos (Supplementary Fig. S3), demonstrating that Exos encapsulation could help to protect more miRNAs from being degraded at −80 °C for more than 7 days. To prove that RVG-cluster 3-Exos could home to injured kidneys, we characterized the tissue biodistribution of injected Exos through in vivo imaging. DiD-labeled RVG-cluster 3-Exos and unmodified cluster 3-Exos were injected into *db/db* mice intravenously via the tail vein. After 12 h, the dissected organs were harvested and examined under the IVIS Spectrum imaging system (Supplementary Fig. S4). As shown in Fig. 2f, renal DiD fluorescence was significantly increased in the group treated with RVG-cluster 3-Exos compared with the unmodified cluster 3-Exo group. Consistently, qRT–PCR revealed higher expression of miR-23a-3p, miR-26a-5p, and miR-27a-3p in the RVG-cluster 3-Exo-treated kidney (Fig. 2g). Therefore, these data revealed that our strategy of delivering cluster 3 using RVG-Exos enhanced both the stability and kidney targeting.

RVG-cluster 3-Exos protected against TIF in mice with DN

To evaluate the therapeutic efficacy of RVG-cluster 3-Exos for TIF, *db/db* mice at 12 weeks of age were intravenously administered Exos (100 μg) once a week for 8 weeks until they were sacrificed at 20 weeks of age (Supplementary Fig. S5). The exogenously added RVG-cluster 3-Exos replenished miR-23a-3p, miR-26a-5p and miR-27a-3p in the kidney of the *db/db* mice (Fig. 3a). Elevated sCr and 24 h urinary protein levels were markedly ameliorated by RVG-cluster 3-Exo treatment (Fig. 3b). To fully assess the efficacy of RVG-cluster 3-Exos, we performed PAS and Masson staining of kidney sections. The results showed that vacuolar degeneration of tubules and TIF were obviously mitigated in the RVG-cluster 3-Exo-treated group (Fig. 3c). Moreover, immunofluorescence staining revealed that α-SMA was expressed at lower levels in the RVG-cluster 3-Exo-treated group, accompanied by decreased expression of Kim-1 (Fig. 3d). In addition, the mRNA expression levels of α-SMA, collagen I, Fibronectin, E-cadherin, and Kim-1 were reversed by RVG-cluster 3-Exo treatment, consistent with the Western blot results (Fig. 3e, f). These data suggested that RVG-cluster 3-Exos alleviated TIF in DN.

RVG-cluster 3-Exos inhibit the accumulation of extracellular matrix (ECM) in TECs

Considering that TECs play a critical role in driving the progression of TIF in DN, manifested in the secretion of a large amount of ECM, and miR-23a-3p, miR-26a-5p, and miR-27a-3p were primarily expressed in the proximal tubules (Fig. 1f), we hypothesized that RVG-cluster 3-Exos protect against TIF by inhibiting TEC-mediated ECM accumulation. First, we examined the uptake of RVG-cluster 3-Exos by TECs. As expected, we found that there was an increase in the internalization of DiD-labeled RVG-cluster 3-Exos in TECs (Fig. 4a), indicating that DiD-labeled RVG-cluster 3-Exos were transfected into TECs. Moreover, RVG-cluster 3-Exos transfection reversed the reduced miR-23a-3p, miR-26a-5p, and miR-27a-3p expression in TECs, which was caused by HG administration (Fig. 4b), indicating that Exos were successfully internalized by TECs and exhibited potential effective targeting to TECs. Furthermore,

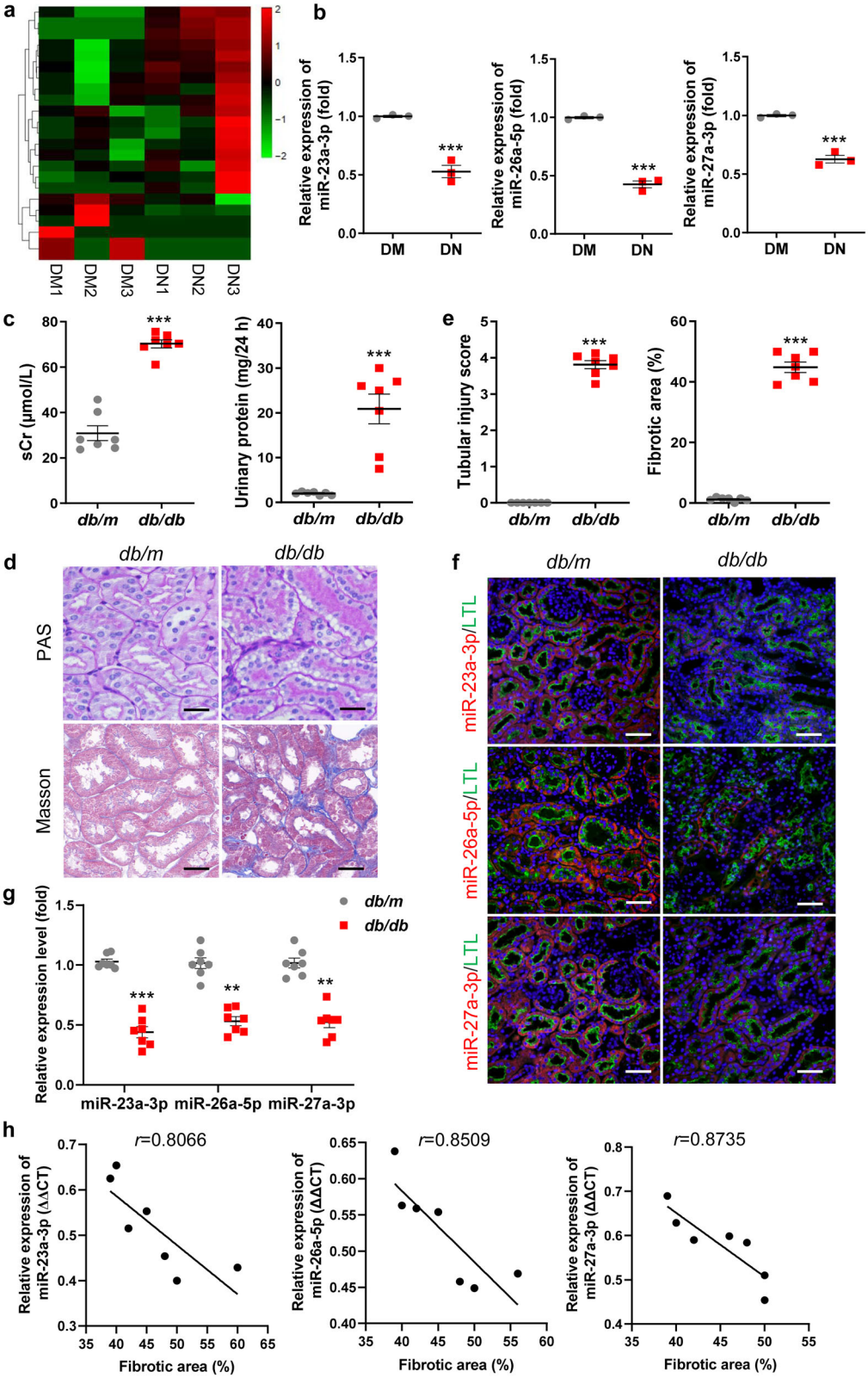

Fig. 1 Downregulated miR-23a-3p, miR-26a-5p, and miR-27a-3p were associated with TIF in DN. a The hierarchical clustering heatmap shows differentially expressed miRNAs in serum samples of patients with DM and DN. **b** MiR-23a-3p, miR-26a-5p, and miR-27a-3p were validated by qRT–PCR, with U6 as a normalization control. **c** sCr and 24 h urinary protein levels in the mice with DN at 20 weeks of age. $n = 7$ per group. **d** Representative images of PAS and Masson staining of the renal cortex. Scale bars, 20 μm. **e** Quantification of tubular injury and TIF based on PAS and Masson staining. $n = 7$ per group. **f** FISH analysis of miR-23a-3p, miR-26a-5p and miR-27a-3p in kidney tissues. Scale bars, 50 μm. **g** qRT–PCR analysis of miR-23a-3p, miR-26a-5p, and miR-27a-3p expression in kidney tissues. **h** Correlation analysis between miR-23a-3p ($P = 0.0284$), miR-26a-5p ($P = 0.0152$), and miR-27a-3p ($P = 0.0102$) and TIF in the mice with DN. $^{**}P < 0.01$, $^{***}P < 0.001$. Cluster 3, miR-23a/27a/26a cluster; DM, diabetes mellitus; DN, diabetic nephropathy; LTL, lotus tetragonolobus lectin; sCr, serum creatinine.

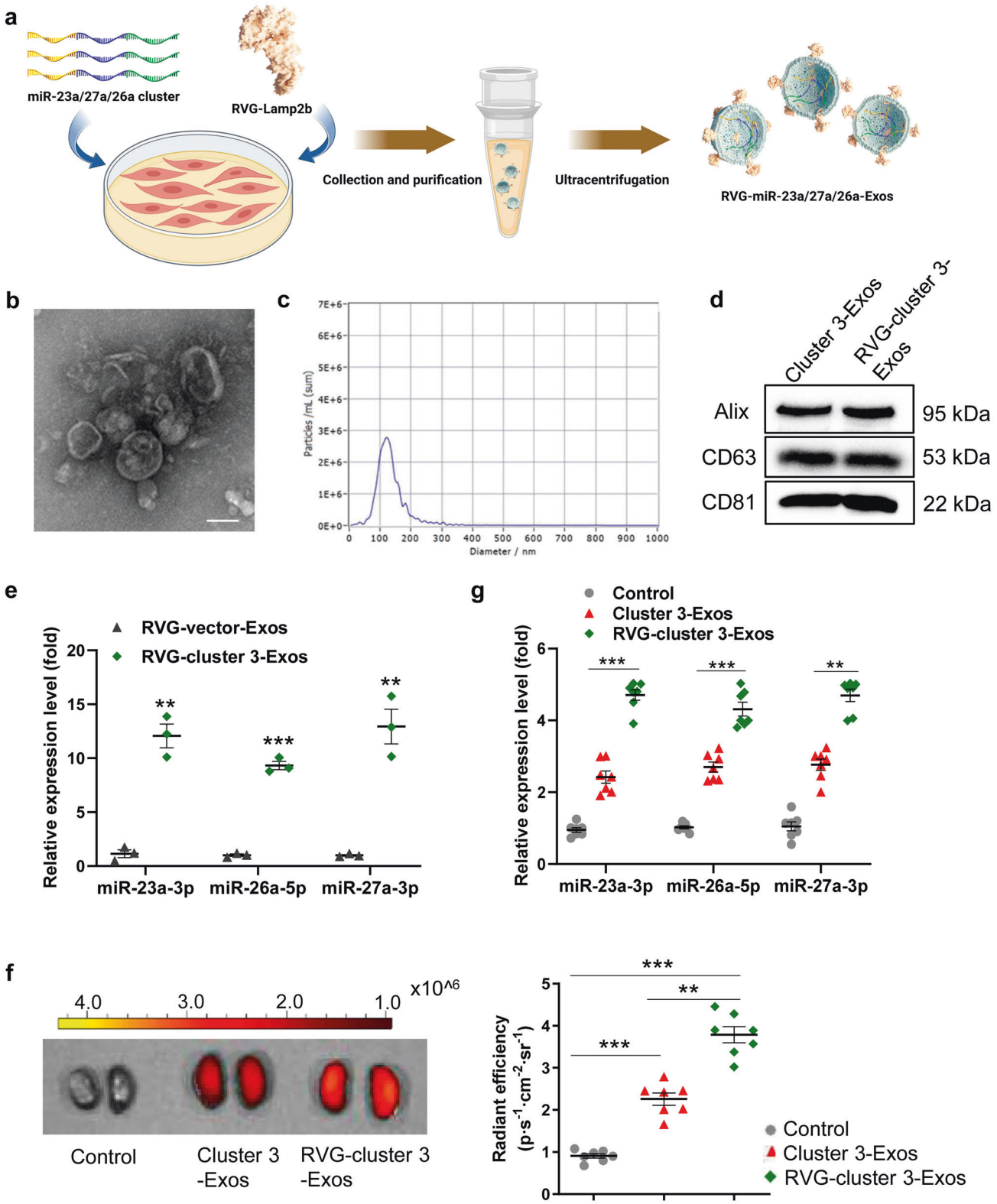

Fig. 2 Engineered RVG-modified Exos homing to injured kidneys. a Schematic representation of the production and harvest of engineered Exos encapsulating the cluster 3 with RVG peptide. Image was drew using BioRender.com. **b** Morphology of RVG-Exos under TEM. Scale bars, 100 nm. **c** Representative NTA validation of the size distribution of RVG-Exos. **d** Western blot analysis of exosomal marker proteins (Alix, CD63, and CD81). **e** qRT–PCR analysis of miR-23a-3p, miR-26a-5p and miR-27a-3p expression in the *db/db* mice treated with RVG-miR-23a/27a/26a-Exos. The results are normalized to U6. **f** Imaging of fluorescence intensity in the db/db mice after intravenous injection of RVG-miR-23a/27a/26a-Exos or miR-23a/27a/26a-Exos. **g** qPCR analysis of miR-23a-3p, miR-26a-5p and miR-27a-3p expression in the kidney after intravenous injection of RVG-miR-23a/27a/26a-Exos and miR-23a/27a/26a-Exos. $^{**}P < 0.01$, $^{***}P < 0.001$. Exo, exosome; RVG, rabies virus glycoprotein.

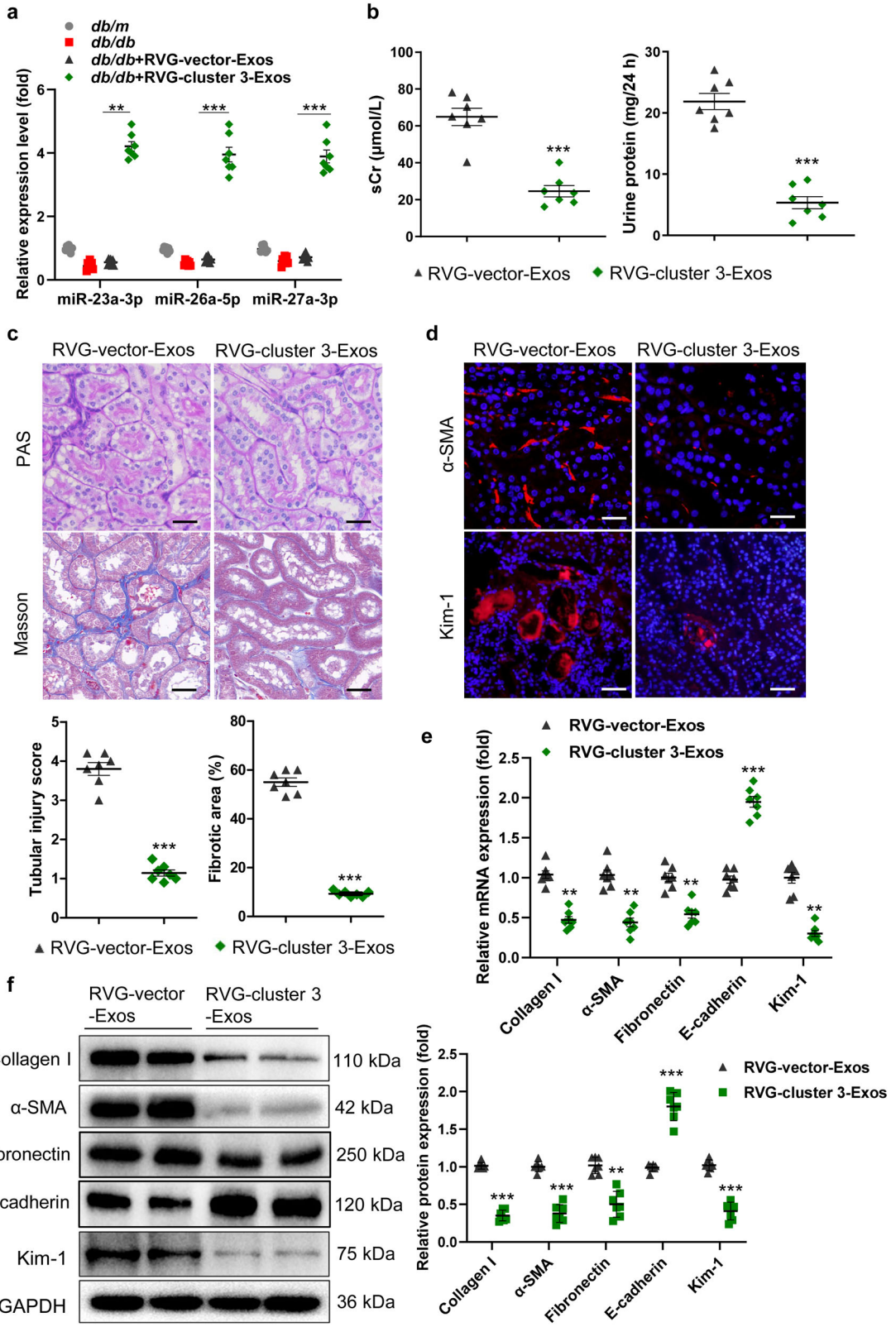

Fig. 3 RVG-miR-23a/27a/26a-Exos attenuate TIF in the mice with DN. At 12 weeks of age, *db/db* mice were intravenously administered Exos (100 μg) once a week for 8 weeks until they were sacrificed at 20 weeks of age. **a** The expression of miR-23a-3p, miR-26a-5p and miR-27a-3p in the kidney were assayed by qRT–PCR. The results are normalized to U6. $n = 7$ per group. **b** sCr and 24 h urinary protein levels. $n = 7$ per group. **c** Representative images of PAS and Masson staining of the renal cortex. Scale bars, 20 μm. **d** Representative images of α-SMA and Kim-1 immunostaining. Scale bars, 20 μm (α-SMA). Scale bars, 50 μm (Kim-1). **e, f** qRT–PCR and Western blot analyses of α-SMA, collagen I, Fibronectin, E-cadherin, and Kim-1 expression. The relative levels were normalized to GAPDH. $n = 7$ per group. $^{**}P < 0.01$, $^{***}P < 0.001$. α-SMA, α-smooth muscle actin; Kim-1, kidney injury molecule-1; TIF, tubulointerstitial fibrosis.

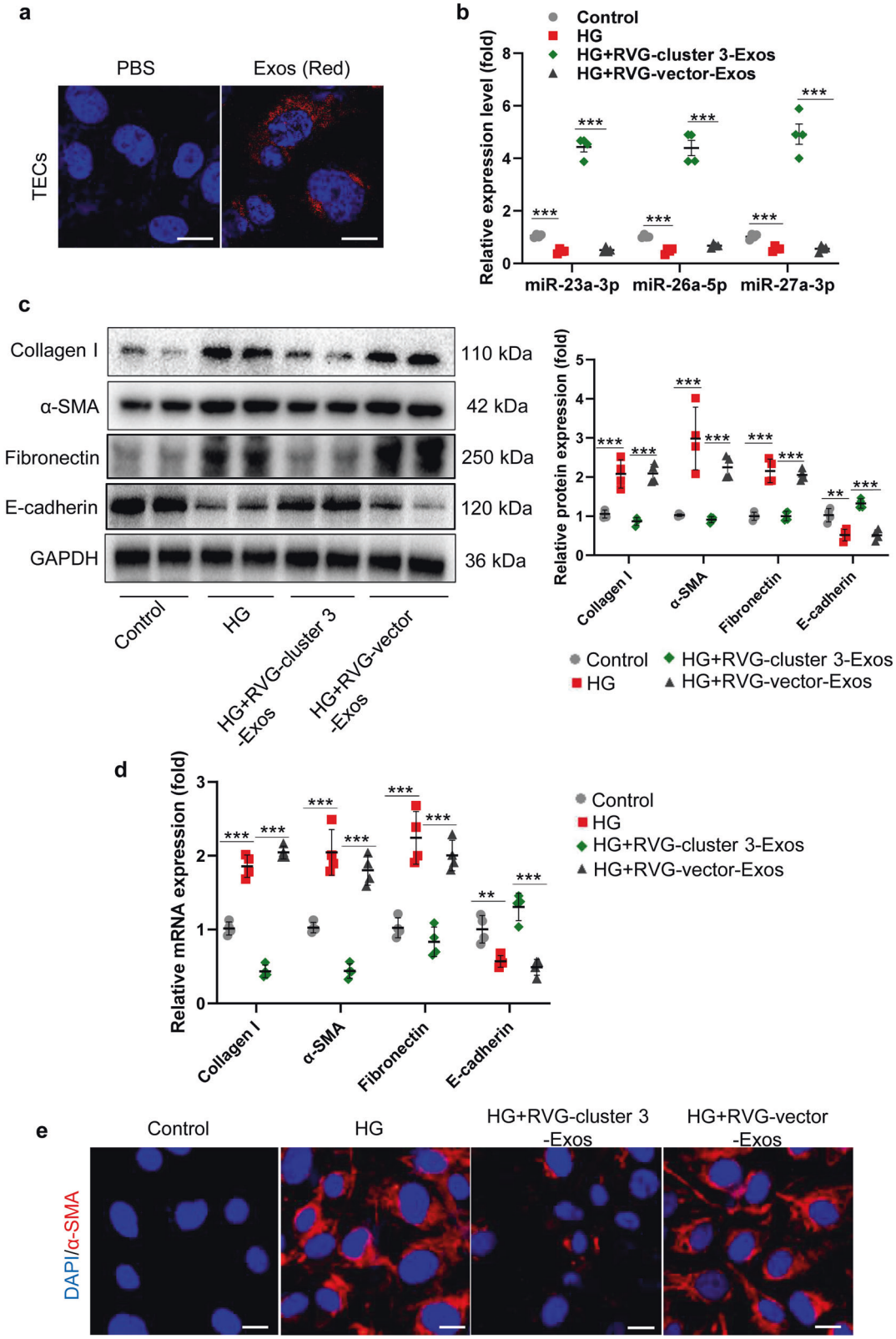

Fig. 4 RVG-miR-23a/27a/26a-Exos inhibit ECM accumulation in HG-treated TECs. (**a**) Representative fluorescent images show the uptake of DiD-labeled RVG-miR-23a/27a/26a-Exos by HG-treated TECs. Scale bars, 10 μm. (**b**) The expression of miR-23a-3p, miR-26a-5p and miR-27a-3p in the HG-treated TECs treated with RVG-miR-23a/27a/26a-Exos. The relative levels were normalized to U6. (**c**, **d**) Western blot and qRT–PCR analyses of α-SMA, collagen-1, Fibronectin, and E-cadherin expression. The relative levels were normalized to GAPDH. (**e**) Representative images of α-SMA immunostaining. Scale bars, 10 μm. $^{**}P < 0.01$, $^{***}P < 0.001$. HG, high glucose.

Western blot and qRT–PCR analyses validated that RVG-cluster 3-Exos could dramatically inhibit the synthesis of fibrosis-related proteins (α-SMA, collagen I, Fibronectin) and increase the expression of E-cadherin in TECs (Fig. 4c, d). In addition, immunofluorescence showed that the expression of α-SMA was reduced by RVG-cluster 3-Exo treatment (Fig. 4e). Thus, these results collectively demonstrated that RVG-cluster 3-Exos could ameliorate the progression of TEC-mediated ECM deposition.

Synergistic antifibrotic activity of RVG-cluster 3-Exos in mice with DN

To investigate whether the miRNA cluster is superior in the treatment of TIF, we examined the therapeutic effects of miR-23a/27a or miR-26a alone. Then, RVG-miR-23a/27a-Exos and RVG-miR-26a-Exos were established following the same methods. First, the expression levels of miR-23a-3p, miR-26a-5p, and miR-27a-3p among each group were detected in kidneys from *db/db* mice (Supplementary Fig. S6a). As shown in Fig. 5a–d, compared to that of the group with RVG-miR-23a/27a-Exo or RVG-miR-26a-Exo treatment, decreased sCr and 24 h urinary protein levels were accompanied by improved vacuolar degeneration of tubules and lower TIF histologically in the mice with DN treated with RVG-cluster 3-Exos. Moreover, immunofluorescence revealed that RVG-cluster 3-Exo treatment could decrease the levels of α-SMA and Kim-1 compared to that of the group with single RVG-miR-23a/27a-Exo or RVG-miR-26a-Exo treatment (Fig. 5e). Moreover, qRT–PCR and Western blot analysis revealed that RVG-cluster 3-Exos were better than RVG-miR-23a/27a-Exos or RVG-miR-26a-Exos alone in reducing the expression of α-SMA, collagen I, and Kim-1 in the TIF treatment (Fig. 5f, g and Supplementary Fig. S6b).

Then, the synergistic anti-ECM accumulation of RVG-cluster 3-Exos in TECs was explored. As presented in Supplementary Fig. S7a, the qRT–PCR results demonstrated lower expression levels of α-SMA and collagen I in the RVG-cluster 3-treated group than in the RVG-miR-23a/27a-Exo-treated or RVG-miR-26a-Exo-treated group. A similar expression pattern was shown by Western blot analysis and immunofluorescence (Supplementary Fig. S7b, c). Collectively, these data indicated that RVG-cluster 3-Exos exert synergistic antifibrotic activity in DN.

RVG-cluster 3-Exos exert antifibrotic activity by targeting multiple genes

To explore the exact molecular mechanisms of the synergistic antifibrotic activity of RVG-cluster 3-Exos, we performed mRNA-seq analysis to compare differentially expressed targets in the HG-stimulated TECs treated with RVG-cluster 3-Exos, RVG-miR-23a/27a-Exos or RVG-miR-26a-Exos, as displayed by the hierarchical clustering heatmap (Fig. 6a). Moreover, bioinformatics databases (including miRDB and TargetScan) were used to clarify the underlying downstream target genes. Interestingly, we found that miR-23a-3p and miR-26a-5p commonly targeted Lpp, miR-27a-3p targeted Zbtb20, and miR-26a-5p targeted Klhl42, which were predicted to be the potential molecular mechanisms of the antifibrotic activity of RVG-cluster 3-Exos (Fig. 6b). First, we examined their expression levels and location in vivo. qRT–PCR analysis showed that the levels of Lpp, Zbtb20, and Klhl42 were significantly increased in the DN group. However, RVG-cluster 3-Exo treatment resulted in lower expression of Lpp than single RVG-miRNA-Exo administration. As expected, RVG-miR-23a/27a-Exos or RVG-miR-26a-Exos alone could only reduce the expression of the specific target genes Zbtb20 and Klhl42, respectively (Fig. 6c). A similar expression pattern was also confirmed by Western blot (Fig. 6d) and immunohistochemistry analysis (Fig. 6e). In addition, the exact mechanisms of RVG-cluster 3-Exos in anti-ECM accumulation in TECs under HG stimulation were demonstrated in vitro (Supplementary Fig. S8a, b).

To further explore the direct targets of cluster 3, we performed a luciferase reporter analysis of cultured HEK293T cells using a reporter construct in which the luciferase coding sequence was fused to the 3′UTR (position 3476–3483nt) of mouse Lpp (miR-23a-3p/Lpp-3′UTR) and the 3′UTR (position 1792–1799nt) of mouse Lpp (miR-26a-5p/Lpp-3′UTR). As expected, the luciferase activity of Lpp was markedly repressed by miR-23a-3p and miR-26a-5p, indicating that Lpp is a direct target of both miR-23a-3p and miR-26a-5p (Fig. 6f, Supplementary Fig. S8c,d). Furthermore, we found that miR-26a-5p markedly repressed luciferase activity in the cells transfected with Klhl42-3′UTR (position 146–153nt), and miR-27a-3p markedly repressed luciferase activity in the cells transfected with Zbtb20-3′UTR (position 20233-20239nt) (Fig. 6f, Supplementary Fig. S8e, f). These data showed that Zbtb20 is a direct target of miR-27a-3p and that Klhl42 is a direct target of miR-26a-5p.

Collectively, these data demonstrated that RVG-cluster 3-Exo treatment played a synergistic antifibrotic role in DN progression not only by potentiating the effect on the common target but also by expanding the effect on specific single target.

Inhibition of Lpp ameliorated the progression of TIF in DN

To investigate the contributions of Lpp to TIF progression in vivo, we used AAV injection via the tail vein to knock down Lpp expression in the mice with DN (Supplementary Fig. S9). The efficiency of Lpp downregulation in tubules from the renal cortex was evaluated by qRT–PCR, Western blot and immunohistochemistry. The results showed that Lpp expression was significantly decreased in mice, and representative images showed that proximal renal tubules were stained with specific antibodies against Lpp (Fig. 7a–c). Loss of Lpp effectively decreased the sCr levels and 24 h urinary protein (Fig. 7d). Importantly, tubule injury, vacuolar degeneration and TIF were markedly diminished in the kidneys of the AAV-Lpp RNAi-injected mice with DN, as evidenced by PAS and Masson staining (Fig. 7e). Furthermore, immunofluorescence showed that silencing Lpp markedly reversed the expression of α-SMA and Kim-1 in the mice with DN (Fig. 7f). Moreover, knockdown of Lpp reversed the transcript and protein levels of α-SMA, collagen I, Fibronectin, E-cadherin, and Kim-1 (Fig. 7g and Supplementary Fig. S10). Thus, the downregulation of Lpp dramatically relieved the progression of TIF in DN. Together, these results demonstrated that Lpp played a critical role in the pathophysiology of DN and that inhibition of Lpp significantly ameliorated the progression of TIF in DN.

DISCUSSION

The global prevalence of DN is estimated to be approximately 40% in patients with DM and still has an annual upwards trend. Increased evidence has demonstrated that TIF plays a crucial role underlying this process. Although various important advances in the molecular mechanisms of TIF have been made, there is no targeted therapy to prevent TIF progression. In this study, our results demonstrated a promising approach of delivering more miR-23a/27a/26a clusters by Exos from muscle satellite cells to injured kidneys and assessed the efficacy of exogenous miR-23a/27a/26a clusters in improving TIF in DN. Surprisingly, delivery of the miR-23a/27a/26a cluster by Exos could enhance the stability of the miR-23a/27a/26a cluster and ameliorate TIF by a mechanism that synergistically targets several profibrotic regulators (Fig. 8).

Numerous studies have shown that miRNAs are involved in regulating the pathophysiology of DN; however, the mechanisms of action are still unclear. At present, the regulation of complex cellular pathways by single miRNAs remains limited. The concept of miRNA clusters has not been previously explored in DN and may provide a novel strategy for clinical translation. In our study, we found that miR-23a-3p, miR-26a-5p, and miR-27a-3p, coexpressed in a module of the miRNA cluster, have a strong negative correlation with TIF in DN, which indicated that the

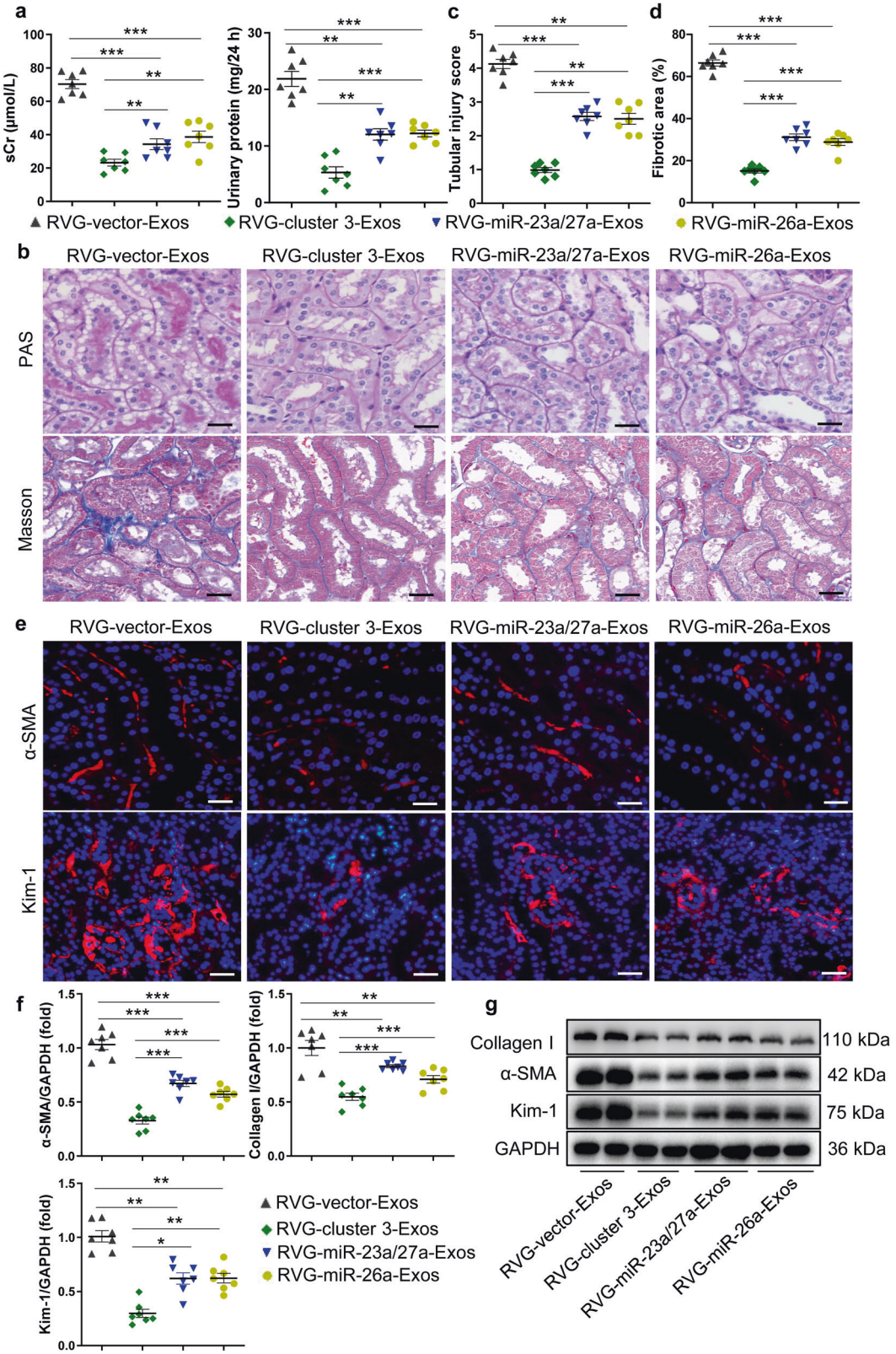

Fig. 5 Synergistic antifibrotic activity of RVG-miR-23a/27a/26a-Exos in mice with DN. a Effects of RVG-miR-23a/27a/26a-Exos, RVG-miR-23a/27a-Exos and RVG-miR-26a-Exos on sCr and 24 h urinary protein of the mice with DN. **b** Representative images of PAS and Masson staining of the renal cortex. Scale bars, 20 μm. **c, d** Quantification of tubular injury and TIF based on PAS and Masson staining. $n = 7$ per group. **e** Representative images of α-SMA and Kim-1 immunostaining. Scale bars, 20 μm (α-SMA). Scale bars, 50 μm (Kim-1). **f, g** qRT–PCR and Western blot analyses of α-SMA, collagen-1, and Kim-1 expression. The relative levels were normalized to GAPDH. $^{*}P < 0.05$, $^{**}P < 0.01$, $^{***}P < 0.001$.

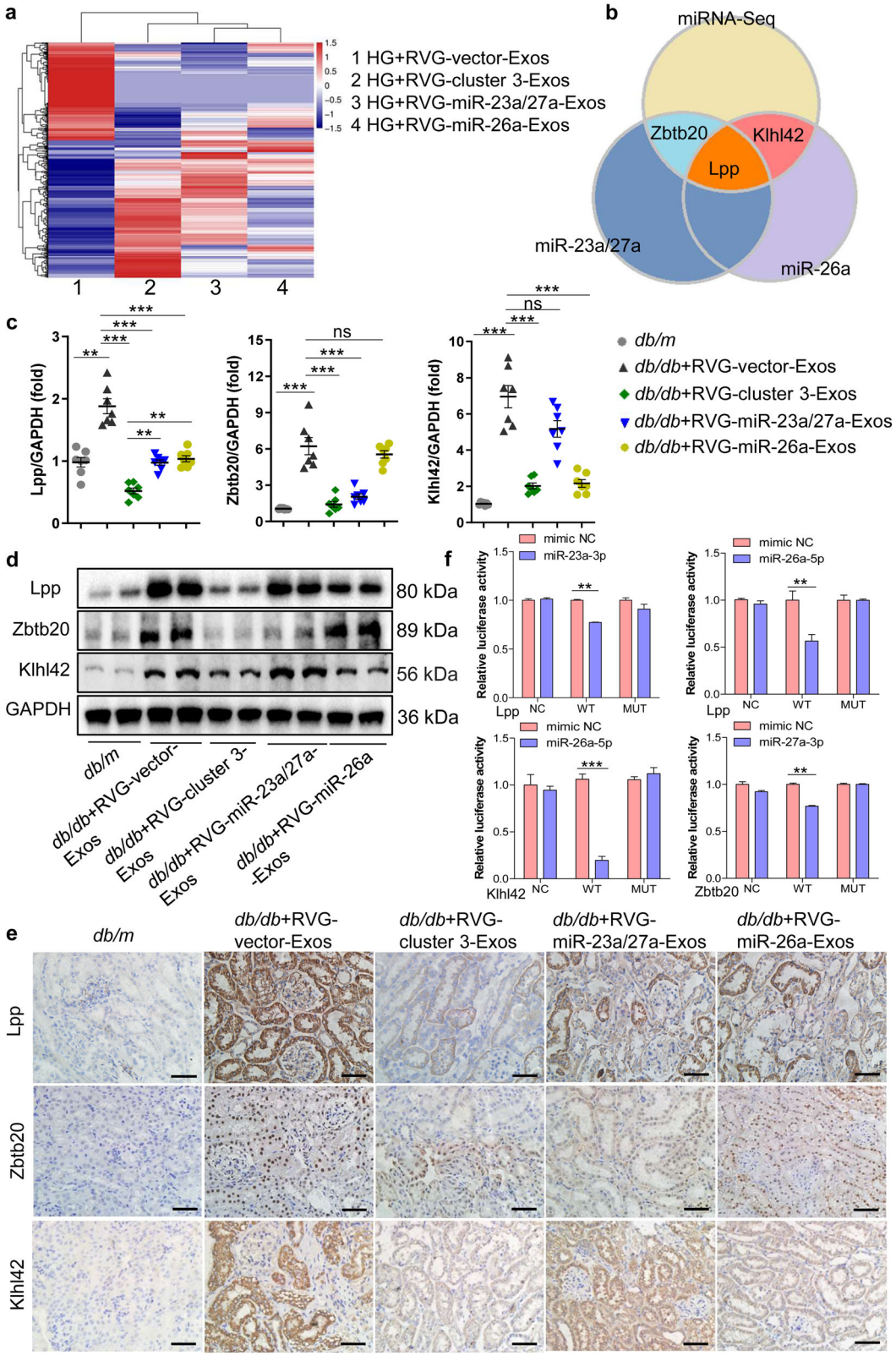

Fig. 6 RVG-cluster 3-Exos exert antifibrotic activity by targeting multiple genes. a Heatmap showing differentially expressed targets identified by RNA-seq in the TECs treated with RVG-vector-Exos (1), RVG-miR-23a/27a/26a-Exos (2), RVG-miR-23a/27a-Exos (3) or RVG-miR-26a-Exos (4) under HG conditions. **b** Intersection analysis of the RNA-seq, TargetScan and miRDB databases. **c** qRT–PCR verified the relative expression levels of Lpp, Zbtb20 and Klhl42 in different groups in vivo. $n = 7$ per group. **d** Western blot analysis of Lpp, Zbtb20 and Klhl42 in vivo. $n = 7$ per group. **e** Immunohistochemistry confirmed the location of Lpp, Zbtb20 and Klhl42 in the kidney and the relative expression in vivo. Scale bars, 50 μm. **f** Luciferase reporter assays identified Lpp as a target in common of miR-23a-3p and miR-26a-5p, Klhl42 as a target of miR-26a-5p and Zbtb20 as a target of miR-27a-3p. $n = 3$ per group. $^{**}P < 0.01$, $^{***}P < 0.001$. ns, no significant difference; NC, negative control; WT, wild type; MUT, mutant; Lpp, lipoma-preferred partner; Zbtb20, Zinc finger and BTB domain containing 20; Klhl42, Kelch-like protein 42.

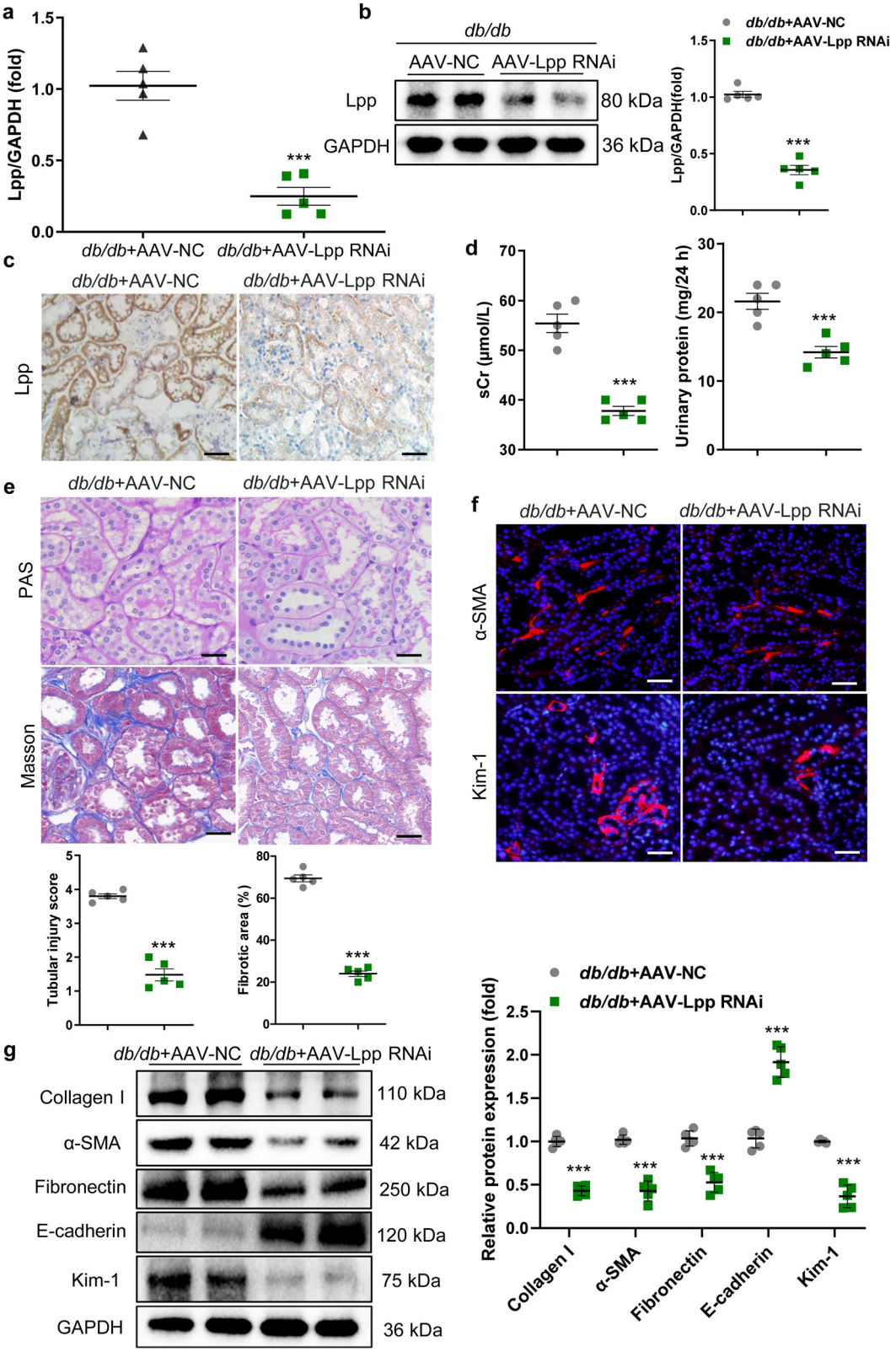

Fig. 7 Inhibition of Lpp contributes to the recovery of TIF in the mice with DN. a–c The efficiency of Lpp knockdown in tubules from the renal cortex was evaluated by qRT–PCR, Western blot and immunohistochemistry. Scale bars, 50 μm. **d** sCr and 24 h urinary protein levels in DN with AAV-vector or AAV-Lpp RNAi. The relative levels were normalized to that of GAPDH. **e** Representative images of PAS and Masson staining after AAV-Lpp RNAi administration. Scale bars, 20 μm. **f** Representative images showing the kidney sections stained with specific antibodies against α-SMA and Kim-1. Scale bars, 50 μm (α-SMA). Scale bars, 20 μm (Kim-1). **g** Representative Western blot and quantitative data of renal α-SMA, collagen I, Fibronectin, E-cadherin, and Kim-1 protein expression. $^{**}P < 0.01$, $^{***}P < 0.001$. AAV, adeno-associated virus.

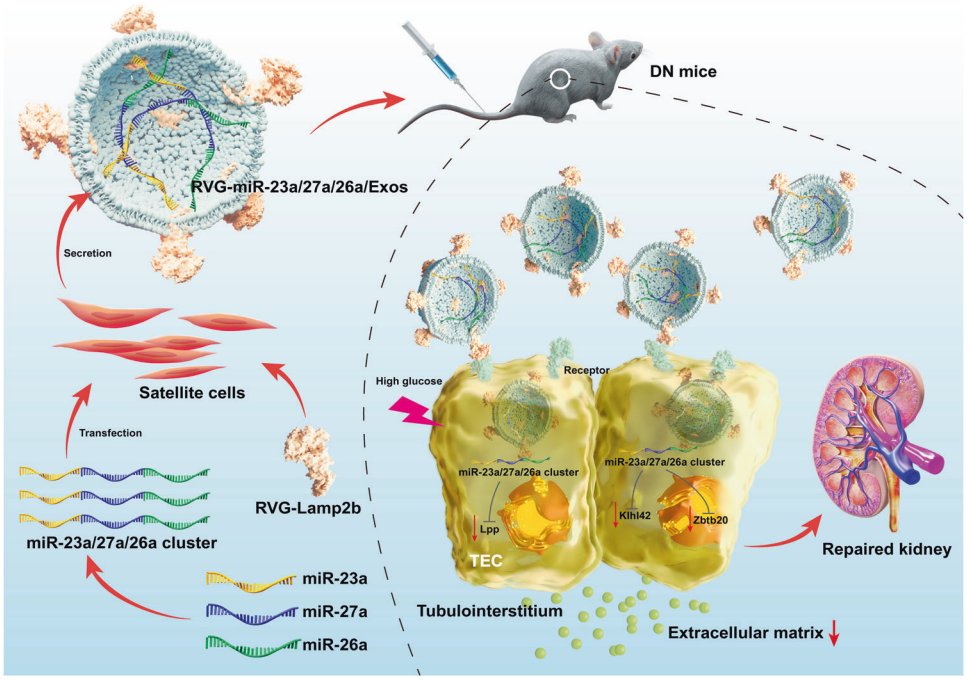

Fig. 8 Schematic illustration of RVG-miR-23a/27a/26a-Exos for the treatment of DN. Delivery of miR-23a/27a/26a cluster by RVG-modified satellite cell-derived Exos could be a promising targeted treatment for DN. RVG-miR-23a/27a/26a-Exos could effectively ameliorate tubular injury and TIF by a mechanism that synergistically targets several profibrotic regulators, which not only regulated miRNA cluster-targeting Lpp simultaneously, but controlled miR-27a-3p-targeting Zbtb20 and miR-26a-5p-targeting Klhl42, respectively. miR-23a, miR-23a-3p; miR-26a, miR-26a-5p; miR-27a, miR-27a-3p.

miR-23a/27a/26a cluster may be explored as a novel and more effective therapy for DN. Previous studies reported that miRNAs could regulate several diseases through multiple pathways [34, 35], among which the canonical pathway is involved in post-transcriptional regulation of gene expression by binding to the 3′UTR of their target messenger RNAs (mRNAs) to suppress expression [36]. In our study, we found that the miR-23a/27a/26a cluster could regulate several genes that are relevant to fibrotic processes. MiR-26a-5p targets Klhl42, and miR-27a-3p targets Zbtb20. Lpp is the common target of miR-23a-3p and miR-26a-5p. Studies have revealed that Lpp, Zbtb20 and Klhl42 are associated with heart and liver fibrosis [37–39]; however, no study has reported the relationship with renal fibrosis. Our data showed that Lpp, Zbtb20 and Klhl42 were located in the proximal tubule, and their high expression levels were reversed by overexpressing miR-23a/27a/26a in the mice with DN, indicating that they may play important roles in DN. Additionally, the mRNA and protein expression of Lpp, whose mRNAs are targeted simultaneously by miR-23a-3p and miR-26a-5p, was incrementally decreased with the full cluster compared to the single miRNA, suggesting that the biological effect of the miRNA cluster not only expands the targetome but also potentiates the effect on common targets. Our results revealed that using clustered miR-23a/27a/26a as a treatment for preventing renal fibrosis in DN is significantly more effective and feasible than single miRNA-mediated therapy.

However, there remain many challenges in applying miRNAs as therapeutics because of the easy degradation in circulation and incomplete delivery to target organs [40, 41]. Recently, convincing evidence has shown that Exos derived from stem cells can be used as miRNA or drug delivery vehicles for disease therapeutics [42, 43]. Our previous studies have shown that skeletal muscle satellite cell-derived exosomes were able to treat muscle atrophy and renal fibrosis in kidney disease models because of their low immunogenicity and favorable safety profile [24, 33], which provides evidence for the existence of a beneficial crosstalk system between skeletal muscle and kidneys. In our study, it was confirmed that skeletal muscle satellite cell-derived exosomes could deliver the miR-23a/27a/26a cluster as nanocarriers to improve kidney impairment and attenuate TIF.

Owing to the low targeting of Exos to kidneys and their easy uptake by other organs, we developed a method to successfully deliver the miR-23a/27a/26a cluster to injured kidneys based on engineered Exos. We transfected Adv-RVG-Lamp2b into muscle satellite cells to increase the efficacy of intravenously delivered Exos. Studies have shown that RVG can direct Exos to organs that express the acetylcholine receptor, such as the kidney [44]. Moreover, Lamp2b is primarily expressed on the surface of Exos and can bring targeting peptides (e.g., RVG) to the Exo surface to increase the Exo targeting ability. In our study, we observed a significant increase in the expression of miR-23a-3p, miR-26a-5p and miR-27a-3p in the RVG-modified Exo group compared with the unmodified Exo group in the mice with DN, which confirmed that RVG-modified exosomes could deliver more materials to home to the kidneys.

To sum up, we have constructed a platform for targeted delivery of the miR-23a/27a/26a cluster by using muscle satellite cell-derived Exos and highlighted the antifibrotic role of RVG-miR-23a/27a/26a-Exos as a promising nanotherapeutic for DN treatment. Mechanistically, we showed that the miR-23a/27a/26a cluster, as a module of coexpressed microRNAs, could simultaneously target Lpp to potentiate the antifibrotic effect and target Zbtb20 and Klhl42 to expand the ability to ameliorate fibrosis. Our study provides a novel kidney-targeting Exo-based delivery system to manipulate the miR-23a/27a/26a cluster, which could effectively ameliorate TIF in DN, providing a promising therapeutic strategy for DN.

ACKNOWLEDGEMENTS

This work was supported by the National Natural Science Foundation of China (No. 81970664, 82000648, 82070735); the Natural Science Foundation of Jiangsu Province (No. BK20211385, BK20200363); the 789 Outstanding Talent Program of the Second Affiliated Hospital of Nanjing Medical University (No. 789ZYRC202080119,

789ZYRC202090251); the Science and Technology Development Foundation of Nanjing Medical University (No. NMUB2020049) and the Fundamental Research Funds for the Central Universities (No. 2242023K40046). We are grateful for the help provided by Lab Center, the Second Affiliated Hospital of Nanjing Medical University and Institute of Nephrology, Southeast University.

AUTHOR CONTRIBUTIONS

AQZ and BW designed the experiments. JLJ analyzed and interpreted the data and wrote the paper. JLJ, HMS, and ZLL conducted the experiments and analyzed the data. RJ drew the graphical abstract. GTQ, HZ, EW, YYQ, XYL, LD, LCD, and WHG contributed to the data analysis. DFD provided serum samples of patients.

ADDITIONAL INFORMATION

Supplementary information The online version contains supplementary material available at https://doi.org/10.1038/s41401-023-01140-4.

Competing interests: The authors declare no competing interests.

REFERENCES

1. Xue R, Gui DK, Zheng LY, Zhai RN, Wang F, Wang NS. Mechanistic insight and management of diabetic nephropathy: recent progress and future perspective. J Diabetes Res. 2017;2017:1839809.
2. Mori Y, Ajay AK, Chang JH, Mou S, Zhao HP, Kishi SJ, et al. KIM-1 mediates fatty acid uptake by renal tubular cells to promote progressive diabetic kidney disease. Cell Metab. 2021;5:1042–61.
3. Zeni L, Norden AGW, Cancarini G, Unwin RJ. A more tubulocentric view of diabetic kidney disease. J Nephrol. 2017;30:701–17.
4. Lee RC, Feinbaum RL, Ambros V. The C. elegans heterochronic gene lin-4 encodes small RNAs with antisense complementarity to lin-14. Cell. 1993;75:843–54.
5. Cerqueira DM, Tayeb M, Ho J. MicroRNAs in kidney development and disease. JCI Insight. 2022;7:e158277.
6. Wonnacott A, Denby L, Coward RJM, Fraser DJ, Bowen T. MicroRNAs and their delivery in diabetic fibrosis. Adv Drug Deliv Rev. 2022;182:114045.
7. Vinas JL, Spence M, Porter CJ, Douvris A, Gutsol A, Zimpelmann JA, et al. microRNA-486-5p protects against kidney ischemic injury and modifies the apoptotic transcriptome in proximal tubules. Kidney Int. 2021;100:597–612.
8. Bhaskaran V, Nowicki MO, Idriss M, Jimenez MA, Lugli G, Hayes JL, et al. The functional synergism of microRNA clustering provides therapeutically relevant epigenetic interference in glioblastoma. Nat Commun. 2019;10:442.
9. Diazzi S, Baeri A, Fassy J, Lecacheur M, Marin-Bejar O, Girard CA, et al. Blockade of the pro-fibrotic reaction mediated by the miR-143/145 cluster enhances the responses to targeted therapy in melanoma. EMBO Mol Med. 2022;14:e15295.
10. Nilsen A, Hillestad T, Skingen VE, Aarnes EK, Fjeldbo CS, Hompland T, et al. miR-200a/b/-429 downregulation is a candidate biomarker of tumor radioresistance and independent of hypoxia in locally advanced cervical cancer. Mol Oncol. 2022;16:1402–19.
11. Kalluri R, LeBleu VS. The biology, function, and biomedical applications of exosomes. Science. 2020;367:eaau6977.
12. Zhang Y, Bi JY, Huang JY, Tang YN, Du SY, Li PY. Exosome: a review of its classification, isolation techniques, storage, diagnostic and targeted therapy applications. Int J Nanomed. 2020;15:6917–34.
13. Yim N, Ryu SW, Choi K, Lee KR, Lee S, Choi H, et al. Exosome engineering for efficient intracellular delivery of soluble proteins using optically reversible protein–protein interaction module. Nat Commun. 2016;7:12277.
14. Yang TZ, Martin P, Fogarty B, Brown A, Schurman K, Phipps R, et al. Exosome delivered anticancer drugs across the blood-brain barrier for brain cancer therapy in Danio rerio. Pharm Res. 2015;32:2003–14.
15. Tang TT, Wang B, Wu M, Li ZL, Feng Y, Cao JY, et al. Extracellular vesicle–encapsulated IL-10 as novel nanotherapeutics against ischemic AKI. Sci Adv. 2020;6:eaaz0748.
16. Kim S, Lee SA, Yoon H, Kim MY, Yoo JK, Ahn SH, et al. Exosome-based delivery of super-repressor IkBa ameliorates kidney ischemia-reperfusion injury. Kidney Int. 2021;100:570–84.
17. Wang B, Wang J, He W, Zhao YJ, Zhang AQ, Liu Y, et al. Exogenous miR-29a attenuates muscle atrophy and kidney fibrosis in unilateral ureteral obstruction mice. Hum Gene Ther. 2020;31:367–75.
18. Cao JY, Wang B, Tang TT, Wen Y, Li ZL, Feng ST, et al. Exosomal miR-125b-5p deriving from mesenchymal stem cells promotes tubular repair by suppression of p53 in ischemic acute kidney injury. Theranostics. 2021;11:5248–66.
19. An Y, Lin SY, Tan XJ, Zhu S, Nie FF, Zhen YH, et al. Exosomes from adipose-derived stem cells and application to skin wound healing. Cell Prolif. 2021;54:e12993.
20. Liu YJ, Guo Y, Bao SM, Huang HD, Liu WH, Guo WK. Bone marrow mesenchymal stem cell-derived exosomal microRNA-381-3p alleviates vascular calcification in chronic kidney disease by targeting NFAT5. Cell Death Dis. 2022;13:278.
21. Hu XM, Shen N, Liu AQ, Wang WD, Zhang LH, Sui ZG, et al. Bone marrow mesenchymal stem cell-derived exosomal miR-34c-5p ameliorates RIF by inhibiting the core fucosylation of multiple proteins. Mol Ther. 2022;30:763–81.
22. Sacco A, Doyonnas R, Kraft P, Vitorovic S, Blau HM. Self-renewal and expansion of single transplanted muscle stem cells. Nature. 2008;456:502–6.
23. Menasche P. Skeletal muscle satellite cell transplantation. Cardiovasc Res. 2003;58:351–7.
24. Wang HD, Wang B, Zhang AQ, Hassounah F, Seow YQ, Wood M, et al. Exosome-mediated miR-29 transfer reduces muscle atrophy and kidney fibrosis in mice. Mol Ther. 2019;27:571–83.
25. ADA. Chronic kidney disease and risk management: standards of medical care in diabetes-2022. Diabetes Care. 2022;45:175–84.
26. Lee SM, Bressler R. Prevention of diabetic nephropathy by diet control in the *db/db* mouse. Diabetes. 1981;30:106–11.
27. Sharma K, McCue P, Dunn SR. Diabetic kidney disease in the *db/db* mouse. Am J Physiol Ren Physiol. 2003;284:1138–44.
28. Luo CW, Zhou S, Zhou ZM, Liu YH, Yang L, Liu JF, et al. Wnt9a promotes renal fibrosis by accelerating cellular senescence in tubular epithelial cells. J Am Soc Nephrol. 2018;29:1238–56.
29. Qu GT, He TT, Dai AS, Zhao YJ, Guan D, Li SW, et al. miR-199b-5p mediates adriamycin-induced podocyte apoptosis by inhibiting the expression of RGS10. Exp Ther Med. 2021;22:1469.
30. Zhang AQ, Wang HD, Wang B, Yuan YG, Klein JD, Wang XH. Exogenous miR-26a suppresses muscle wasting and renal fibrosis in obstructive kidney disease. FASEB J. 2019;33:13590–601.
31. Cui MY, Yao XX, Lin Y, Zhang D, Cui RJ, Zhang XW. Interactive functions of microRNAs in the miR-23a-27a-24-2 cluster and the potential for targeted therapy in cancer. J Cell Physiol. 2020;235:6–16.
32. Zhang AQ, Li M, Wang B, Klein JD, Price SR, Wang XH. miRNA-23a/27a attenuates muscle atrophy and renal fibrosis through muscle-kidney crosstalk. J Cachexia Sarcopenia Muscle. 2018;9:755–70.
33. Wang B, Zhang C, Zhang AQ, Cai H, Price SR, Wang XH. MicroRNA-23a and MicroRNA-27a mimic exercise by ameliorating CKD-Induced muscle atrophy. J Am Soc Nephrol. 2017;28:2631–40.
34. Wang B, Zhang AQ, Wang HD, Klein JD, Tan L, Du J, et al. miR-26a limits muscle wasting and cardiac fibrosis through exosome-mediated microRNA transfer in chronic kidney disease. Theranostics. 2019;9:1864–77.
35. Dragomir MP, Knutsen E, Calin GA. Classical and noncanonical functions of miRNAs in cancers. Trends Genet. 2022;38:379–94.
36. Dragomir MP, Knutsen E, Calin GA. SnapShot: unconventional miRNA functions. Cell. 2018;174:1038.
37. Hooper CL, Dash PR, Boateng SY. Lipoma preferred partner is a mechanosensitive protein regulated by nitric oxide in the heart. FEBS Open Bio. 2012;2:135–44.
38. Li FF, Du MM, Yang YM, Wang Z, Zhang H, Wang XY, et al. Zinc finger and BTB domain-containing protein 20 aggravates angiotensin II-induced cardiac remodeling via the EGFR-AKT pathway. J Mol Med (Berl). 2022;100:427–38.
39. Lear TB, Lockwood KC, Larsen M, Tuncer F, Kennerdell JR, Morse C, et al. Kelch-like protein 42 is a profibrotic ubiquitin E3 ligase involved in systemic sclerosis. J Biol Chem. 2020;295:4171–80.
40. He L, Thomson JM, Hemann MT, Mu D, Goodson S, Powers S, et al. A microRNA polycistron as a potential human oncogene. Nature. 2005;435:828–33.
41. Gao ZQ, Zhu XL, Dou YX. The miR-302/367 cluster: a comprehensive update on its evolution and functions. Open Biol. 2015;5:1501–38.
42. Yang JL, Zhang XF, Chen XJ, Wang L, Yang GD. Exosome mediated delivery of miR-124 promotes neurogenesis after ischemia. Mol Ther Nucleic Acids. 2017;7:278–87.
43. Cai GF, Cai GL, Zhou HC, Zhuang Z, Liu K, Pei SY, et al. Mesenchymal stem cell-derived exosome miR-542-3p suppresses inflammation and prevents cerebral infarction. Stem Cell Res Ther. 2021;12:2.
44. Seow YQ, Wood MJ. Biological gene delivery vehicles: beyond viral vectors. Mol Ther. 2009;17:767–77.